Bulletin of Earthquake Engineering
https://doi.org/10.1007/s10518-024-01918-9

ORIGINAL ARTICLE

# A ductile seismic design strategy for the cross-aisle direction of racking systems

**Dimitrios Tsarpalis[1] · Dimitrios Vamvatsikos[1] · Agnese Natali[2] · Francesco Morelli[2] · Filippo Delladonna[3] · Emanuele Vantusso[4]**

Received: 2 May 2023 / Accepted: 5 April 2024


**Abstract**
Due to their lightness and simple connectivity, steel racking systems are typically considered as "low-dissipative" structures, which is reflected in the modern seismic codes by the absence of capacity design and the adoption of low behaviour factors. This limited capability of stress redistribution significantly increases the vulnerability of racks under beyond-design seismic hazards and raises the demand for more resilient designs. Along these lines, the proposed Plastic Ovalization Strategy (POS) attempts to increase the ductility of the individual upright frames comprising the cross-aisle direction of racks, and at the same time to preserve their low-cost and easy-to-assemble nature. This is achieved by tasking the bearing failure mechanism of the diagonal bolt hole to absorb seismic deformations, while capacity design is employed to keep the rest of the structure in the elastic zone. Following a detailed discussion on the motives and basic principles of the strategy, two high-rise racking systems are designed twice by professional engineers, once using standard approaches and then by additionally employing the proposed POS rules. Finally, the two design solutions are compared by conducting a comprehensive seismic assessment, which employs a phenomenological macro-model comprising elastic elements and nonlinear springs to simulate the bearing failure mechanism.

**Keywords** Steel racking systems · Bearing failure · Ductile seismic design · Cross-aisle direction

✉ Dimitrios Tsarpalis
dimitrists93@central.ntua.gr

[1] Institute of Steel Structures, School of Civil Engineering, National Technical University of Athens, 9, Iroon Polytechneiou Str., Zografou Campus, 15780 Athens, Greece

[2] Department of Civil Engineering, University of Pisa, Pisa, Italy

[3] Head Office Design Department, SACMA S.P.a. Industrial Rackings and Plants, Sandigliano, Italy

[4] Technical Department, MODULBLOK S.P.a. Industrial Rackings and Plants, Pagnacco, Italy

Published online: 09 May 2024

## 1 Introduction

Steel pallet racking systems are civil engineering structures used to store goods and materials inside a warehousing unit. The high importance of warehousing facilities to the logistics sector raises the demand for racking structures that are resilient to extreme hazards. A disruption to the supply chain, or even worse, a destruction of stockpiled goods, can lead to economic losses that are far greater than the initial cost of the supporting rack. Such phenomena were reported during the Emilia-Romagna (Italy) earthquake (Galli et al. 2012), where several racks experienced severe damages or even collapsed.

To facilitate different logistics needs, a variety of racking systems has arisen over the years with significant diversity, not only from a logistics standpoint but also in terms of structural behaviour (Tsarpalis et al. 2022). As a result, racks may range from a series of independent low/mid/high-rise substructures inside the warehouse like the prolific adjustable pallet racking (APR) systems, up to integrated solutions of automated rack supported warehouses (ARSWs, see Fig. 1). ARSWs play a dual static role by supporting both the pallets and the cladding/façade of the warehouse, bypassing the need for the construction of heavy (and thus expensive) steel trusses to form the external supporting shell. Moreover, they offer automated solutions for the handling process of the pallets, thus minimizing human intervention and improving the exploitation of the available footprint by reducing the required aisles (Tsarpalis et al. 2021b). At the same time, due to their high-density nature, local failures can propagate to the entire warehouse and initiate a global failure mechanism.

Both for conventional APRs and newer ARSWs, two main directions are typically defined to efficiently describe their geometric configuration: the down-aisle direction, which is parallel to the aisles of the warehouse and, perpendicularly to the former, the cross-aisle direction. Figure 2 illustrates examples of the cross- and down-aisle views for the two most common ARSWs typologies, namely the automated double-depth cranes and the automated multi-depth shuttles. Double-depth cranes (Fig. 2b) belong to direct-access systems and provide easy accessibility to the pallets, stored with a maximum number of two units for each row in the cross-aisle direction, but decrease the use of the available footprint of the warehouse by needing more aisles. On the other hand, multi-depth shuttles (Fig. 2c) are more compact systems that maximize the storage density, while losing accessibility to the pallets that are stored in long storage tunnels serviced by mechanized shuttles running on rails; this renders them more suitable for handling a reduced number of stock keeping units.

**Fig. 1** Example of a high-rise ARSW in the construction stage (photo courtesy of SACMA S.p.a.)

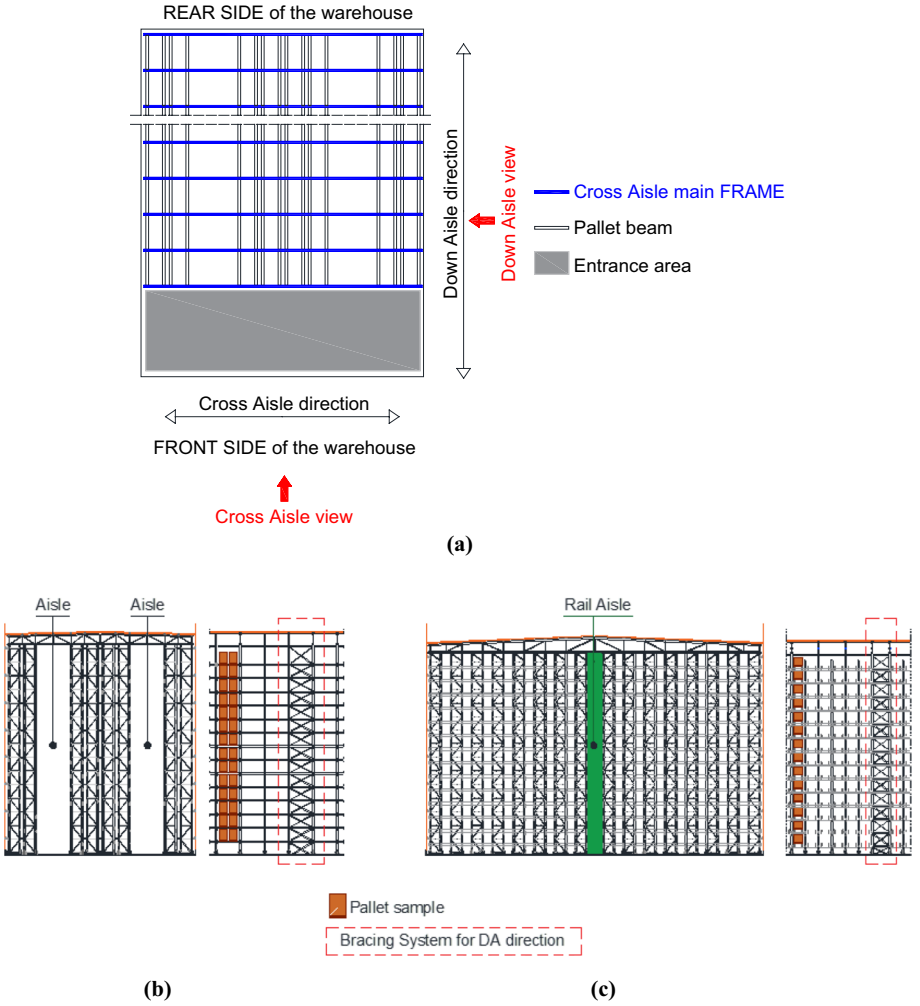


**Fig. 2** Typical **a** plan view of an ARSW, **b** cross- and down-aisle views of a double-depth ARSW, and **c** the cross- and down-aisle views of a multi-depth ARSW

From a structural point of view, most rack typologies share a common design philosophy in terms of steel profiles, connections, and lateral load-resisting systems. Typically, thin-walled cold-formed profiles are used. Along the down-aisle direction the pallets are accommodated by the so-called pallet beams, which are hooked or bolted to the uprights (i.e., columns) of the system to form a flexible moment resisting frame (MRF). When this loose upright-to-beam connection is combined with high number of load levels, the MRF is usually not capable of adequately limiting the stability coefficient (e.g., per ASCE/SEI 7-22 2022; EN 1998-1 2004), rendering the structure susceptible to P-Δ phenomena. To tackle this issue, high-rise racks typically comprise a stiff bracing system along their down-aisle direction, either by introducing bracing towers at the two ends of the structure or by placing a series of braces at selected down-aisle frames. The cross-aisle direction is always realized by a set of upright frames, which are braced

frames that comprise two (or even three) uprights connected along their height with a bracing system. At the ground level, the upright frames are connected to the foundation floor by an anchorage system, while in ARSWs they are also bolted to the roof truss at their top.

Currently, racks are seismically designed according to modern rack-specific guidelines, such as EN 16681 (2016) and RMI (2012). These are an improvement vis-à-vis seismic design standards for conventional steel structures, such as the Eurocodes, which were never meant for rack applications (Caprili et al. 2018). Still, strictly speaking, EN 16681 and RMI are applicable only to APRs, lacking the needed modifications to respect the structural idiosyncrasies and nonconventional geometry of ARSWs. For example, Natali et al. (2022a) and Kondratenko et al. (2022) have shown that the "low-dissipative" approach of at least EN 16681 (2016), using low behaviour factors ($q$) of e.g., 1.5, results to ARSWs that are prone to brittle failure modes, such as upright buckling, base connection failure (e.g., concrete cone failure), and bolt shear failure; this is the case even under design-level seismic loads. While in some case studies the ductile bearing failure mechanism was prevalent (Natali et al. 2022a), still the designed racks demonstrated limited stress redistribution capability, as the absence of proper capacity design resulted in early failures on the uprights. By taking also into account the additional uncertainties in the definition of the design seismic loads due to the introduction of several reduction factors (Natali et al. 2022a, 2022b, 2022c), there is presently significant interest in finding innovative solutions to reduce the vulnerability of racks under earthquake excitations.

One straightforward option to enhance the seismic resilience is a brute-force increase of strength by using heavier, and thus stronger, steel sections. This can be achieved at the global level, either by directly increasing the design seismic forces (e.g., by using the 10% in 50 years design spectrum instead of the 20% in 50 years), or by reducing the behaviour (or strength reduction or response modification) factor to increase the safety margin. While such approaches can help a rack to safely resist higher hazards, they do not guard against disproportionate impact due to local brittle failures, and as such they can be problematic for rare events with higher return periods. Indeed, modern seismic design codes like EN 1998-1 (2004), do not recommend adopting a low-dissipative approach when designing steel structures in high seismicity areas, as the lack of load redistribution means that a local failure of a component can initiate the complete collapse of the structure.

A time-honoured and more agile approach to this problem is to increase the ductility of the rack, by exploiting the plastic behaviour of certain components, while keeping the rest of the structure in the elastic zone by enforcing capacity design (Tsarpalis et al. 2020). However, such a design strategy is a novelty for racks and should respect the philosophy of the industry, which demands thin-walled steel sections with very simple bolted/hooked connections, minimizing the effort during the installation and disassembly process.

To enhance the seismic behaviour of the racks along the down-aisle direction, an intuitive solution is to reinforce the bracing towers, by directly adopting capacity design rules similar to those of braced frames in typical steel buildings (Brandonisio et al. 2012). As found by Kondratenko et al. (2022), the bracing towers, being far stiffer than the weak MRF formed by the pallet uprights and beams, accumulate almost the entire seismic base shear of the structure. This comes very handy for the development of a reliable plastic failure mechanism, as one may apply the costly rules of capacity design only on few parts of the structure, herein the bracing towers. Thus, the accumulated experience in the design of conventional buildings can be employed to ensure the ductile behaviour of the stiff bracing towers, e.g. using heavier hot-rolled sections and associated connections, while the typical cold-formed profiles can be used for the more flexible pallet uprights and beams.

On the other hand, the achievement of a plastic mechanism along the cross-aisle direction is a more challenging task, as the seismic loads are distributed almost evenly along the individual upright frames (Tsarpalis et al. 2021b; Natali et al. 2022d). This means that one has to increase the ductility of all upright frames in order to develop a global ductile behaviour. As the upright frames are basically braced frames, a potential source of ductility are the diagonals. However, the diagonal-to-upright bolted connection is typically realized with only one M10 or M12 (i.e., of 10 mm or 12 mm diameter, respectively) normal shear bolt, potentially with two shear planes to increase the connection resistance, as illustrated in Fig. 3. As a result, the resistance of the connection (e.g., bearing strength or bolt shear resistance) is not sufficiently high to allow the diagonal member to yield and enter the nonlinear zone. Per the authors' experience in racking technology, the creation of an over-resistant diagonal-to-upright connection that would resolve the aforementioned issue requires the introduction of additional bolts, plates, or precision cutting procedures that complicate the installation process and it is, therefore, not convenient in terms of costs (Natali and Morelli 2023).

Herein, a simpler solution of seismic improvement is investigated, the so-called plastic ovalization strategy (POS), which relies on the plastic ovalization of the diagonal bolt holes to keep all brittle failure mechanisms at bay. Similar concepts have been employed in lightweight steel constructions e.g., in steel frame wall systems composed of thin-walled framing members with plane or corrugated steel sheets (Stojadinovic and Tipping 2007; Vigh et al. 2013, 2014; Fülöp and Dubina 2004; Landolfo 2019). POS is expected to increase the overall ductility of the upright frames, at least by a limited amount until laboratory testing verification and associated system analyses are performed (e.g., see Vamvatsikos et al. 2020), without necessarily aiming to achieve the high q-factors, e.g., of 4.0 (Brandonisio et al. 2012), typical of hot-rolled steel braced frames. On the positive side,

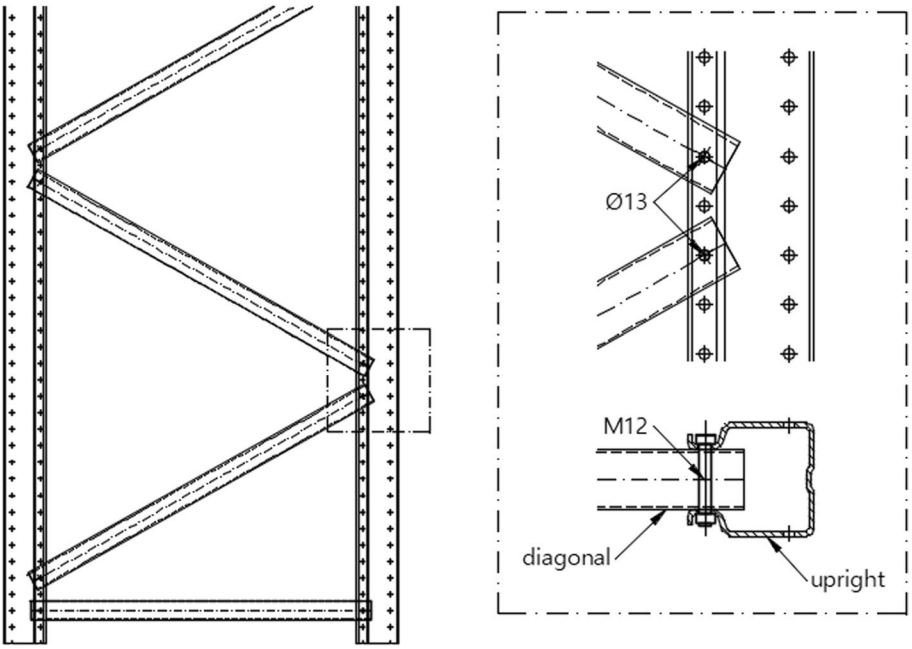


**Fig. 3** Typical diagonal-to-upright bolted connection, using an M12 bolt with two shear planes

it does not require an over-resistant diagonal-to-upright connection, while less-demanding capacity design rules can be employed (e.g., preventing fragile failures in the diagonal element or connection to the upright). Moreover, as diagonal buckling is avoided thanks to the weaker plastic ovalization mechanism, the typical "D-type" bracing can be used (see Fig. 3), allowing designers and manufactures to stay within their comfort zone in terms of design and construction practices.

In the following, the theoretical framework of POS is delineated by (a) conceptualizing the basic principles and motives behind the strategy, (b) proposing new capacity design rules to accomplish the desired ductile behaviour, and (c) comparing the performance of POS to more traditional approaches. While it is recognized that experimental tests are essential for the calibration of the actual behaviour of the diagonal-to-upright connection, a preliminary numerical model is proposed for the nonlinear simulation of the bearing failure mechanism, using empirical relationships available in the literature. To demonstrate the impact of the proposed POS rules to the seismic behaviour of racks, the cross-aisle direction of one double- and one multi-depth ARSW is examined. Each racking system is designed by professional engineers twice: first by using the standard EN16681 approach and then by additionally employing the POS rules. Finally, a comprehensive seismic assessment is conducted to compare the seismic performance of the two design solutions employing state-of-the-art assessment methods.

## 2 Theoretical concept and design rules

### 2.1 Failure modes of a bolted shear connection

Being a bolted shear connection, the diagonal-to-upright joint is characterized by the interaction between its constituent bolts and steel plates. Six distinct modes of failure can be identified in such connections (Draganić et al. 2014): (I) end failure, which is further discretized to (Ia) shear, or (Ib) tearing end failure, (II) bearing failure, (III) net section failure, (IV) bolt failure, (V) block tear-out failure, and (VI) bolt pull-through failure (Fig. 4). On the other hand, the current European (EN 1993-1-8 2005) and American (ANSI/AISC 360-16 2016) specifications, aggregate the six failure modes of a bolted shear connection to only four mechanisms: (1) block tear out failure, (2) bearing failure, (3) net section failure, and (4) bolt shear failure. Essentially, they combine Modes (Ia) and (V) into mechanism (1), while Modes (Ib) and (VI) are considered to be covered by the resistance of mechanism (2), the bearing failure (Draganić et al. 2014; Može and Bek 2014).

From all six modes, Mode (II), the bearing failure, is considered to be the most ductile. Indeed, pure bearing involves the plastic ovalization of the bolt holes, allowing for large deformations of the connection, to as much as the bolt diameter before material rupture (Kiymaz 2009). However, excessive hole elongations might lead to impractical displacements and, thus, they need to be controlled under the service loads (Kiymaz 2009). According to EN 1993-1-8 (2005) provisions, the bearing resistance of a steel plate is influenced mostly by the proximity of the plate hole to the plate boundaries (i.e., the $e_1$ and $e_2$ parameters in Fig. 5), the distance between the adjacent plate holes (i.e., $p_1$ and $p_2$ in Fig. 5) and the additional restraint provided by the nut and bolt head (Kiymaz 2009).

Lately, experimental and analytical studies have showed that the well-known formula of EN 1993-1-8 (2005) underestimates the bearing resistance of a bolted connection (Može et al. 2021). Indeed, the revised prEN 1993-1-8:2021 (2021) proposes a new formula for

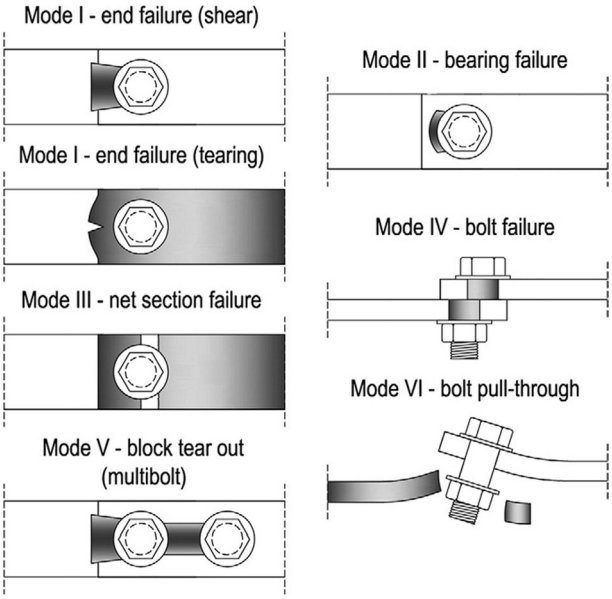


**Fig. 4** Failure modes on a bolted shear connection (Draganić et al. 2014)

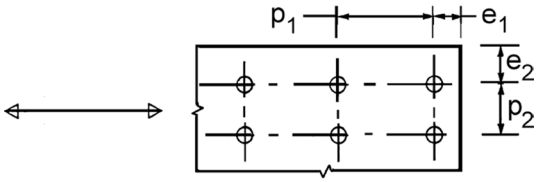


**Fig. 5** Edge and inner distances of a bolt layout according to EN 1993-1-8 (2005)

the bearing resistance that depends on the relative end-distance $e_1$ / $d_0$ or the spacing between the bolts $p_1$ / $d_0$, while it is independent of the distance perpendicular to the bearing force:

$$F_{b,Rd}^{(2021)} = \frac{k_m \cdot \alpha_b^{(2021)} \cdot f_u \cdot d \cdot t}{\gamma_{M2}} \tag{1}$$

where $F_{b,Rd}^{(2021)}$ is the design bearing resistance per prEN 1993-1-8:2021 (2021), $k_m$ is 1 except for steel grades equal to or greater than S460, for which $k_m$ is 0.9. The coefficient $\alpha_b^{(2021)}$ is given as:

$$\alpha_b^{(2021)} = \begin{cases} \min\left(\frac{e_1}{d_0}, 3 \cdot \frac{f_{ub}}{f_u}, 3\right), & \text{for end bolt} \\ \min\left(\frac{p_1}{d_0} - \frac{1}{2}, 3 \cdot \frac{f_{ub}}{f_u}, 3\right), & \text{for inner bolt} \end{cases} \tag{2}$$

The new formula of the bearing resistance in (1) does not account for distances $e_2$ and $p_2$. Otherwise, the design resistance of the connection is indirectly controlled by the design for block tear out or the net cross-section resistance. Regarding the displacement capacity of the connection, experimental results have demonstrated that the bearing deformation of the bolt hole can be of magnitude of one bolt diameter, $d$ (Kiymaz

2009). Draft prEN 1993-1-8:2021 (2021) provides a method for the calculation of the bearing deformation at bolt holes at or before yielding:

$$\bar{\sigma}_b = \frac{126 \cdot u/d}{\left(1 + \sqrt{30 \cdot u/d}\right)^2} \tag{3}$$

where $\bar{\sigma}_b$ is the normalized bearing stress, $u$ is the embedding of the bolt that causes a local yielding at the edge of the bolt hole, i.e., the bearing deformation. The embedding $u$ is carried out up to 80% of the maximum bearing resistance for grades up to S460 and up to full bearing resistance for S460 and higher grades, as shown in Fig. 6. Afterwards, the stress-deformation relationship is linear (hardening for grades up to S460, perfectly plastic for higher ones) until the achievement of the bolt hole ultimate deformation given by (Može et al. 2021):

$$u_{Xd} = \min\left(\frac{k_m \cdot \alpha_b^{(2021)}}{3}, k_m^2\right) \cdot d \tag{4}$$

Given the normalized bearing stress, $\overline{\sigma}_b$, the bearing force per bolt can be calculated as:

$$F_b(u) = \overline{\sigma}_b(u) \cdot d \cdot t \cdot f_u \tag{5}$$

Even though bearing failure is considered to be ductile on static loading conditions, its cyclic behaviour has not been investigated thoroughly yet. One of the main reasons is that on typical steel structures the bolted connections are designed with overstrength, so that during a seismic event, yielding and buckling of the diagonal braces occurs (or at least it is meant to occur) before any connection failure (EN 1998-1 2004). According to the authors' knowledge, the only available data on the seismic behaviour of bolted connections subject to bearing failure are related to steel corrugated shear wall systems (e.g., Stojadinovic and Tipping 2007; Vigh et al. 2013, 2014). In these studies, it was observed that the failure mechanism was initiated by ovalization of the sheet holes, followed by screw tilt and ultimately pull out, resulting in a pinched hysteretic behaviour.

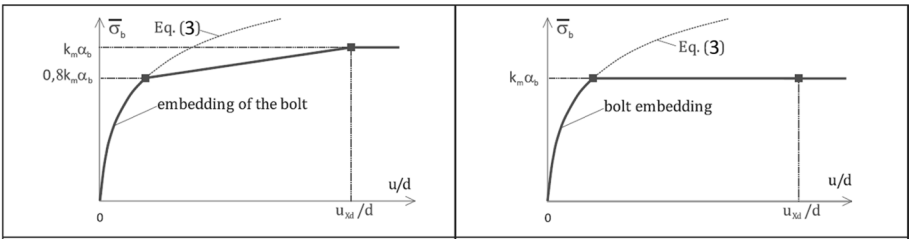


**Fig. 6** Bearing deformation behaviour (adopted from Može et al. 2021)

### 2.2 Proposed capacity design rules

The proposed POS approach relies on the plastic deformation of the diagonal-to-upright bolted connection, mainly due to the elongation of the bolt hole. As mentioned previously, an over-resistant diagonal-to-upright connection may come at odds with the philosophy of the racking structures that prefers simple connections without any additional bolts and plates. As a remedy, POS exploits the ductility of the bearing failure mechanism by employing capacity design rules both in the connections and the members of the upright frame. In the following paragraphs, a set of POS rules is proposed that is suitable for use with EN16681. Still, the same concept can be employed with minor adjustments for use with other guidelines or standards (e.g., RMI 2012). Note that this is certainly not a complete set of rules, as further laboratory testing may reveal additional phenomena that may need to be accounted for, especially for truss configurations other than D-type, to ensure the validity of the capacity design.

#### 2.2.1 Diagonals and diagonal-to-upright connections

The design of the diagonals and the diagonal-to-upright connections shall ensure the occurrence of bearing failure before any other failure mechanism of the diagonal, by adopting the following rules. Note that all resistances below are expressed as the total resistance of the connection, i.e., if a connection has one bolt with two shear planes, $F_{v,Rd}$ is two times the resistance of the bolt in each shear plane:

**POS 1**: The bolt shear resistance ($F_{v,Rd}$) should be 1.20 times greater than the bearing resistance of the diagonal's hole ($F_{b,d,Rd}$):

$$F_{v,Rd} \geq 1.20 \cdot F_{b,d,Rd} \tag{6}$$

**POS 2**: The bearing resistance of the upright's hole ($F_{b,u,Rd}$) should be 1.20 times greater than the bearing resistance of the diagonal's hole ($F_{b,d,Rd}$):

$$F_{b,u,Rd} \geq 1.20 \cdot F_{b,d,Rd} \tag{7}$$

**POS 3**: The net section resistance of the diagonal ($N_{u,Rd}$) should be 1.20 times greater than the member's bearing resistance ($F_{b,d,Rd}$):

$$N_{u,Rd} \geq 1.20 \cdot F_{b,d,Rd} \tag{8}$$

**POS 4**: The buckling resistance of the diagonal ($N_{b,Rd}$) should be 1.20 times greater than the member's bearing resistance ($F_{b,d,Rd}$):

$$N_{b,Rd} \geq 1.20 \cdot F_{b,d,Rd} \tag{9}$$

**POS 5**: The bearing resistance of the diagonal in tension and in compression, $F^{+}_{b,d,Rd}$ and $F^{-}_{b,d,Rd}$, respectively, should not differ by more than 10%. This can be achieved with the introduction of a boltless empty hole in the direction of the load that is adjacent to the bolt hole and away from the member end.

**POS 6**: Rule 8.1.6e of EN 16681 (2016) that governs the design of the diagonals and their connections by multiplying the seismic forces by the behaviour factor of $q$, should be discarded.

**POS 7**: The overstrength factor 1.20 employed in rules POS 1 to POS 4, may be reduced by appropriate testing that ensures the occurrence of bearing strength failure before any other failure mechanism of the diagonal and its connection.

One may notice that capacity rules POS 1 to POS 4 employ a common overstrength factor equal to 1.20; this choice was made to be in accordance with the available regulations for racks, i.e., the rule of EN 16681 (2016) that requests the bolt shear resistance of the diagonal element of the upright frame to be 20% greater than its bearing failure strength. Rules POS 1 and POS 3 are introduced to prevent the brittle bolt shear failure and net section rupture, respectively. Rule POS 2 is meant to ensure that the bolt hole elongation only occurs on the easily replaceable diagonal and does not unduly impact the section of the upright, potentially damaging its buckling capacity. POS 4 protects the diagonal member from abrupt buckling and thus allows designers to employ bracing patterns with non-redundant diagonals, like the typical "D-type" bracing. On the other hand, rule POS 5 is employed to achieve a symmetric cyclic behaviour of the connection, while rule POS 6 aims to reduce the diagonals' overstrength with respect to the connected uprights. Finally, POS 7 is introduced to "reward" structural designers that employ experimental tests to reliably calculate the resistances of the involved members and connections. (see Fig. 7).

### 2.2.2 Non-dissipative elements

The uprights, the horizontal braces, and the roof truss in the case of an ARSW (i.e., the non-dissipative elements) shall be designed to remain in the elastic region under the design seismic loads. This can be achieved by employing the following capacity design rules:

**POS 8**: The uprights should be designed by computing the design axial forces ($N_{Ed}$), shear forces ($V_{Ed}$), and bending moments ($M_{Ed}$) as follows:

$$\begin{aligned} N_{Ed} &= N_{Ed,G} + 1.1 \cdot \gamma_{ov} \cdot \Omega_{min} \cdot N_{Ed,E} \\ M_{Ed} &= M_{Ed,G} + 1.1 \cdot \gamma_{ov} \cdot \Omega_{min} \cdot M_{Ed,E} \\ V_{Ed} &= V_{Ed,G} + 1.1 \cdot \gamma_{ov} \cdot \Omega_{min} \cdot V_{Ed,E} \end{aligned} \tag{10}$$

where $N_{Ed,G}$, $M_{Ed,G}$, and $V_{Ed,G}$ are the compression force, bending moment, and shear force in the upright due to the non-seismic actions included in the combination of actions for the seismic design situation;

$N_{Ed,E}$, $M_{Ed,E}$, and $V_{Ed,E}$ are the compression force, bending moment, and shear force in the upright due to the seismic actions;

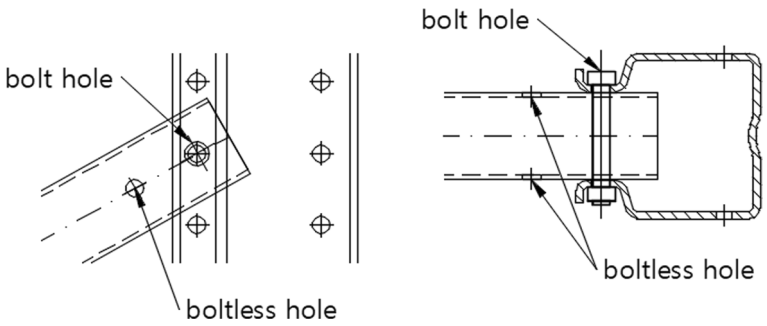


**Fig. 7** Introduction of boltless empty hole adjacent to the bolt hole to satisfy rule POS 5

$\gamma_{ov}$ is the overstrength factor, adopted equal to 1.25 to be in accordance with the EN 1998-1 (2004) provisions. However, its value may be revised given test and supplier data;

$\Omega_{min} = \max\{\Omega_{min,L}, \Omega_{min,U}\}$, and $\Omega_{min,L}$ and $\Omega_{min,U}$ are the minimum overstrengths of the braces connected to the lower and the upper half of upright frame's height, respectively. In other words, first the utilization factor ($UF$) of each diagonal element (including its bolted connection) is computed for the seismic combination at hand. Then, the upright frame is divided into two equal vertical segments and the maximum utilization factors of the lower and the upper half ($UF_{max,L}$ and $UF_{max,U}$, respectively) are calculated. Finally, the minimum overstrengths are computed as $\Omega_{min,L} = 1 \,/\, UF_{max,L}$ and $\Omega_{min,U} = 1 \,/\, UF_{max,U}$.

One may notice that, in tandem with the capacity design rules for typical steel columns, the proposed $\Omega_{min}$ has a constant value along the height of the upright frame. However, in contrast to EN 1998-1 (2004) capacity rules, herein no limitations between the ratio of the maximum and minimum overstrength factors are foreseen (e.g., $\Omega_{max} \,/\, \Omega_{min} \leq 1.2$). This limitation is typically adopted to achieve a uniform distribution of ductility along the height of a braced frame. On the negative side, this would have required to continuously modify the bearing resistance of the diagonals (e.g., by adjusting the distance of the bolt hole to the member end, or the $e_1$ parameter), to achieve a uniform distribution of $\Omega$ s.

The effect of non-uniformity of overstrength on the system capacity may be fairly complex if one seeks to understand the full failure mechanism of the rack. Instead, the proposed simplified concept of $\Omega_{min,L}$ and $\Omega_{min,U}$ for determining overstrength is considered to be adequate for the modest $q$-factor value employed herein. However, it should be stressed that it is a first-guess capacity rule; if the assessment of the case studies designed according to POS reveals weaknesses in the uprights, stricter rules will be required. Finally, as the uprights are typically composed of omega sections with low section modulus, rule POS 8 adds an additional safeguard from early failures by amplifying both the compression forces ($N_{Ed,E}$) and the bending moments ($M_{Ed,E}$) by $1.1{\cdot}\gamma_{ov}{\cdot}\Omega_{min}$.

**POS 9**: The horizontal braces and the roof truss should be designed by computing the design forces and moments as follows:

$$\begin{aligned} N_{Ed} &= N_{Ed,G} + 1.1 \cdot \gamma_{ov} \cdot \Omega_{min} \cdot N_{Ed,E} \\ M_{Ed} &= M_{Ed,G} + M_{Ed,E} \\ V_{Ed} &= V_{Ed,G} + V_{Ed,E} \end{aligned} \tag{11}$$

In contrast to rule POS 8, rule POS 9 does not multiply the design seismic moments and shear forces by the factor of $1.1{\cdot}\gamma_{ov}{\cdot}\Omega_{min}$, as the horizontal braces and the roof elements are usually (a) considered as truss elements that work only axially and (b) under-stressed with respect to the uprights and diagonals. In different configurations where the axial force does not govern the design of the aforementioned members, one should consider including the effect of overstrength on moment and shear demands as well.

### 2.2.3 Base connections

The design of the upright base connections shall ensure the prevention of failure modes on the base plates and the anchorage system. This can be achieved by adopting the following rule:

**POS 10**: The base connections should be designed by multiplying the design base reactions by the $q$-factor used in the seismic design analysis. Additionally, they should be verified

using two scenarios for the gravitational loads: $G + 0.8{\cdot}Q$ and $G + Q$ ($G$ and $Q$ represent the dead and the unit loads, respectively).

The multiplication of the base reactions by $q$ aims to protect the upright base connections from entering the nonlinear range. Regarding the base plate, this includes the prevention of (a) failure of the upright-to-baseplate bolted connection, (b) cracking of the base plate welds, and (c) bending of the base plate. From these three failure modes, mode (c) was examined experimentally and numerically by Tagliafierro et al. (2021) as a promising solution to efficiently reduce the seismic demands when designing new racks or retrofitting existing ones. While the plastic deformation of the base plate under bending demonstrated a ductile monotonic and cyclic behaviour, the allowance of such failures would have violated the basic principles of POS that foresee the upright-to-diagonal connection as the only source of nonlinearity. Still, this does not mean that the two mechanisms cannot be combined in the future.

Regarding the anchorage system, the upright base plates are typically fixed to the concrete slab using post-installed anchors with limited embedment length, facilitating the construction process but rendering the connection prone to brittle failure modes. Indeed, several studies have reported that the concrete cone failure comprises one of the dominant failure modes of ARSWs along their cross-aisle direction (Kondratenko et al. 2022; Natali et al. 2022a). The capacity rule POS 10 aims to prevent such abrupt failures with the obvious cost of requiring anchors with greater diameter and length, which not only increases the weight of the steel used but also complicates the installation procedure due to extensive drilling of the concrete slab.

Finally, the two scenarios for the gravitational loads aim to maximize the uplift forces on the base connections. According to EN 16681 (2016), the design seismic mass of the unit loads is calculated as:

$$M_{E,UL} = R_F \cdot E_{D2} \cdot Q_{P,rated} \tag{12}$$

where $R_F$ is the rack filling grade reduction factor, $E_{D2}$ is the unit load weight modification factor, and $Q_{P,rated}$ is the specified value of the weight of unit loads for the compartment. $E_{D2}$ represents the effects of the interaction between the unit load and the racking structure and will not be discussed further in this study. The $R_F$ reduction factor is related to the occupancy of stored goods in the rack that can be assumed during the seismic event, essentially acting as the $\psi_2$ factor of EN 1998-1 (2004). In contrast to the seismic mass, EN 16681 (2016) does not consider any reduction factors for the definition of the seismic vertical loads, i.e., $R_F$ is equal to 1.0. While this difference between the definition of the masses and vertical loads is ambiguous, it still is on the safe side for the design of the steel members. However, it is not safe for the design of the baseplates and anchors, as high vertical loads result in lower uplift forces. For these reasons, the additional combination "$G + 0.8{\cdot}Q$" was adopted for the gravitational loads along with the code-mandated "$G + Q$", where the 0.8 factor was chosen to reflect the reduced mass recommended by EN16681.

## 3 Numerical validation of proposed design strategy

### 3.1 Seismic design of case studies

To assess the performance of the proposed POS rules, the cross-aisle frames of one double-depth (DD) and one multi-depth (MD) ARSW are examined. These two ARSW archetypes were designed by professional engineers within the context of the European

project STEELWAR (2017), for installation in the city of Van in Turkey. The same design spectrum was adopted for both case studies, comprising a peak ground acceleration of $a_g = 0.3$ g and an importance factor of $\gamma_I = 0.8$. The latter was selected according to EN 16681 (2016) suggestions to (approximately) conform to the 20% in 50 years design spectrum for the design of fully-automated racks. The same norm offers two additional sources of seismic load reduction, the design spectrum modification factors $E_{D1}$ and $E_{D3}$.

The $E_{D1}$ factor is related to the positive effect of pallet sliding that reduces the apparent inertia of the rack (Tsarpalis et al. 2021a) and for the tested structures ended to be equal to 1.0. On the other hand, $E_{D3}$ is used to "*account for the dissipative phenomena that are observed on racks that have suffered earthquakes or tested experimentally, but cannot be described in a mathematical formulation"* and has a default value of 0.8. Depending on the case at hand, this "one fit for all" 0.8 value may or may not include dissipative mechanisms related to the ovalization of the bolt holes. Thus, by adopting an increased $q$-factor while retaining the default value of $E_{D3}$, there is a probability of double-counting the same phenomenon when designing for the POS strategy. However, whether one needs to increase $E_{D3}$ is indeed a question that cannot be answered via a desktop study, only by actual testing. Still, we believe that one can rely upon the same $E_{D3}$ value as this is also used in the down-aisle direction, where this phenomenon is much reduced. For these reasons, both designs adopted the same $E_{D3}$ value of 0.8.

Case study DD has four "macro-columns" of 25.56 m height and 2.35 m width (Fig. 8), where each "macro-column" comprises two K-braced upright frames with mirrored bracing patterns, connected with spacers along their height. Regarding the down-aisle direction (which is not shown here for brevity), the pallet beams are designed to carry two pallets per bay, thus each upright frame carries approximately two pallets per load level. Automated cranes are used for goods handling, operating in 14 load levels: Load levels 1 to 3 are for 1000 kg pallets, 4 to 11 for 800 kg, and 12 to 14 for 600 kg. On the other hand, the cross-aisle direction of case study MD comprises 28 X-braced upright frames of 24.24 m height and 1.14 m width (Fig. 9). MD is designed to carry 9 load levels with four storage cells of 13 unit-load capacity each. Load levels 1 to 2

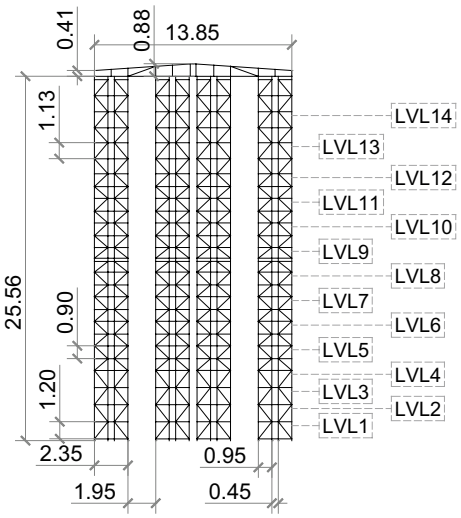


**Fig. 8** Cross-aisle view of case study DD (dimensions in m)

are for 1000 kg pallets, 3 to 5 for 800 kg, and 6 to 9 for 600 kg. The handling process is again fully automated, using cranes and shuttles to deposit and withdraw the pallets.

As already stated, each case study was designed twice by a professional engineer expert in rack structures. First, a "standard" non-ductile design was performed using EN 1993-1-1 (2005), EN 15512 (2009) and EN 16681 (2016), adopting a behaviour factor of $q = 1.5$. Then, the case studies were redesigned according to the new rules POS 1 to POS 10, employing a factor of $q = 1.8$; this value is a preliminary recommendation pending a more accurate evaluation involving numerous experimental and numerical analyses. The following mass combinations were used for both designs: $G + Q$ for the double-depth, and $G + 0.8{\cdot}Q$ for the multi-depth case study, reflecting the lower probability of having any single level filled to full capacity in the considerably wider cross-aisle direction of the multi-depth. The same importance and spectrum modification factors were employed for all cases. All the seismic design assumptions are summarized in Table 1, where "STD" corresponds to the standard, and "POS" to the plastic ovalization design.

Due to the introduction of capacity design rules POS 1 to POS 10, some members and connections of the upright frames had to be modified during the redesign. Table 2 summarizes the major changes in the cross-sections and the bolted connections of the double-depth case study. One may observe that lighter diagonals (30% less material) were used during the POS redesign, mainly due to rule POS 6 that disregards the code-recommended increase of their seismic demand by the q-factor. Moreover, while not imposed by the new design rules, the designer chose to use a single diagonal section in the entire lower half of the structure and a lighter one for the upper half. Each half was further separated into quarters by modifying the $e_1$ parameter. This smooth reduction of the diagonal's resistance along the height of the upright frame is expected to enhance the seismic behaviour of the rack at the cost of slightly complicating erection. On the other hand, the uprights were not modified during the POS design. While rule POS 8 aims to create over-resistant uprights, it is based on a "relaxed" (or more permissible) interpretation of the overstrength factor of EN 1998-1 (2004) and the designer was able to satisfy the capacity checks without increasing the upright section. As a result, the POS design used less steel material with respect to the standard approach (the weight of the steel members composing the cross-aisle direction

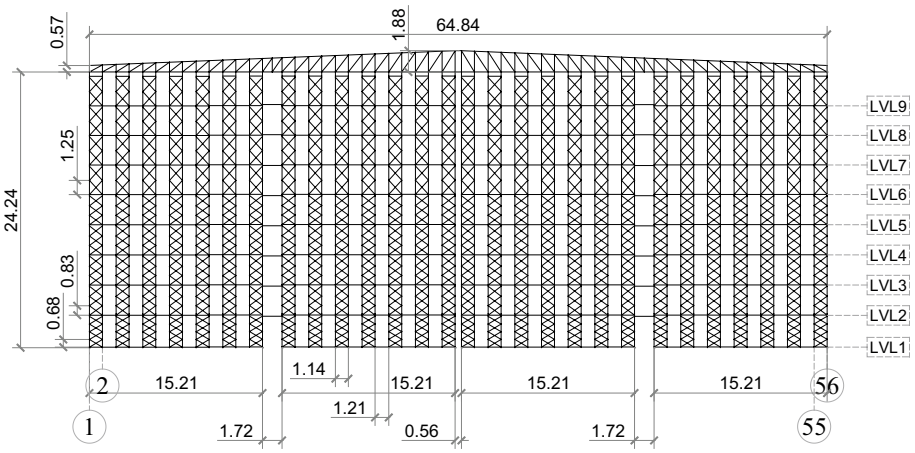


**Fig. 9** Cross-aisle view of case study MD (dimensions in m)

**Table 1** Seismic design assumptions adopted in case studies DD and MD according to the standard design (STD), and the POS redesign (POS)

| | DD-STD | DD-POS | MD-STD | MD-POS |
|---|---|---|---|---|
| $\gamma_I$ | 0.8 | 0.8 | 0.8 | 0.8 |
| $E_{D1}$ | 1.0 | 1.0 | 1.0 | 1.0 |
| $E_{D3}$ | 0.8 | 0.8 | 0.8 | 0.8 |
| $q$ | 1.5 | 1.8 | 1.5 | 1.8 |
| Mass comb | $G$+$Q$ | $G$+$Q$ | $G$+ 0.8·$Q$ | $G$+ 0.8·$Q$ |
| Load comb | $G$+$Q$ | $G$+ $Q$<br>$G$ + 0.8·$Q$* | $G$+$Q$ | $G$+ $Q$<br>$G$ + 0.8·$Q$* |

*For the design of the base connections only, see rule POS 10

**Table 2** Member and connection properties of case study DD according to the standard design (STD), and the POS redesign (POS)

| Member | Height (m) | STD | POS |
|---|---|---|---|
| Uprights | [0.00, 3.73] | Ω + U*: $A = A_1$ | Ω + U: $A = A_1$ |
| | (3.73, 12.58] | Ω**: $A = 0.5 \cdot A_1$ | Ω: $A = 0.5 \cdot A_1$ |
| | (12.58, 25.56] | Ω: $A = 0.32 \cdot A_1$ | Ω: $A = 0.32 \cdot A_1$ |
| Diagonals | [0.00, 6.65] | C***: $A = A_2$<br>$t$ = 3 mm, $e_1$ = 24 mm<br>1M12 8.8 (2 shear planes) | C: $A = 0.7 \cdot A_2$<br>$t$ = 2 mm, $e_1$ = 29 mm<br>1M12 8.8 (2 shear planes) |
| | (6.65, 12.80] | C: $A = A_2$<br>$t$ = 3 mm, $e_1$ = 24 mm<br>1M12 8.8 (2 shear planes) | C: $A = 0.7 \cdot A_2$<br>$t$ = 2 mm, $e_1$ = 22 mm<br>1M12 8.8 (2 shear planes) |
| | (12.80, 18.73] | C: $A = 0.7 \cdot A_2$<br>$t$ = 2 mm, $e_1$ = 24 mm<br>1M12 8.8 (2 shear planes) | C: $A = 0.5 \cdot A_2$<br>$t$ = 1.5 mm, $e_1$ = 23 mm<br>1M12 8.8 (2 shear planes) |
| | (18.73, 25.56] | C: $A = 0.7 \cdot A_2$<br>$t$ = 2 mm, $e_1$ = 24 mm<br>1M12 8.8 (2 shear planes) | C: $A = 0.5 \cdot A_2$<br>$t$ = 1.5 mm, $e_1$ = 15 mm<br>1M12 8.8 (2 shear planes) |
| Anchorage system | – | 4M20 8.8<br>embedment depth: 400 mm | 4M24 8.8<br>Embedment depth: 500 mm |

Section areas are given normalized to the bottommost elements of the STD design

*Ω + U: Ω-type upright section reinforced with a U-type section; **Ω: Ω-type upright section; ***C: channel section with lips

was reduced by 4%, excluding the anchors). Regarding the base connections, rule POS 10 led to a stronger anchorage system with greater anchor diameter and embedment depth.

The effects of the POS rules in MD case study are illustrated in Table 3. Contrarily to the DD example, herein heavier diagonals (+25% more material) were employed during the POS redesign, even though rule POS 6 led to lower design seismic forces. Indeed, in the standard design, the diagonals had slender circular hollow sections (with folded ends to achieve a thickness of 3 mm at the connection), which do not satisfy rule POS 4, i.e., the buckling resistance being greater than the bearing resistance. Thus, in the POS redesign, channel sections with lips were used for the diagonals, with different $e_1$ parameters at the lower and the upper half of the structure. Concerning the uprights, heavier profiles were employed at the POS redesign, but only for the first 2.98 m from the ground. Again, the design rules did not lead to major changes in the uprights, as the designer was able to

**Table 3** Member and connection properties of case study MD according to the standard design (STD), and the POS redesign (POS)

| Member | Height (m) | STD | POS |
|---|---|---|---|
| Uprights | [0.00, 2.98] | Ω + U[a]: $A = A_1$ | Ω + U: $A = 1.79 \cdot A_1$ |
| | (2.98, 13.32] | Ω + U: $A = A_1$ | Ω + U: $A = A_1$ |
| | (13.32, 24.24] | Ω[b]: $A = 0.68 \cdot A_1$ | Ω: $A = 0.68 \cdot A_1$ |
| Diagonals | [0.00, 10.81] | CHS[c]: $A = A_2$<br>$t = 3$ mm, $e_1 = 18$ mm<br>1M8 8.8 (1 shear plane) | C[d]: $A = 1.25 \cdot A_2$<br>$t = 1.5$ mm, $e_1 = 20$ mm<br>1M12 8.8 (1 shear plane) |
| | (10.81, 24.24] | CHS: $A = A_2$<br>$t = 3$ mm, $e_1 = 18$ mm<br>1M8 8.8 (1 shear plane) | C: $A = 1.25 \cdot A_2$<br>$t = 1.5$ mm, $e_1 = 15$ mm<br>1M12 8.8 (1 shear plane) |
| Anchorage system | – | 2M16 8.8<br>embedment depth: 250 mm | 2M20 8.8<br>Embedment depth: 350 mm |

Section areas are given normalized to the bottommost elements of the STD design

[a]Ω + U: Ω-type upright section reinforced with a U-type section; [b]Ω: Ω-type upright section; [c]CHS: circular hollow section; [d]C: channel section with lips

optimize the diagonals instead. In total, the POS redesign resulted in a + 14% increase of steel weight in the cross-aisle direction, excluding the rail beams. Finally, the resistance of the anchors was increased during the POS redesign, having greater diameter and embedment depth.

### 3.2 Preliminary experimental validation of the diagonal connections' behaviour

The cold-formed diagonals adopted in the re-designed case studies were tested under monotonic loads in order to observe the actual behaviour of the connection zone. A diagonal profile is selected from the bottom part of each case study—this being the most stressed under the seismic action—and tested in tension and in compression. The length of each diagonal is 500 mm. Specimens are connected to the universal testing machine through over-resistant connection pieces at their ends, to restrict damage to the diagonal itself (Fig. 10a). When the diagonal is tested under tensile axial force, the parameter influencing bearing resistance should be $e_1$, which is the distance of the hole from the free edge; under compressive force it should be the distance between the connection hole and the boltless one, or $p_1$ (Fig. 10b). The $p_1$ parameter has been evaluated according to POS rule 5, with the aim of having the bearing resistance under compression within 1.1 and 1.0 times the bearing resistance under tension. Elongation of the diagonals is measured through two displacement sensors, and the load is monitored directly through the machine load cell. Table 4 gathers the main characteristics of the tested diagonals, together with the material characterization obtained through coupon tests on the virgin material.

Figure 11 shows the force versus displacement curves obtained for the tested profiles, and Fig. 12 their final configuration. Looking at the force–displacement curves for the two profiles, comparable values of maximum load are obtained, although in the case of the MD one the bearing resistance in compression is more than 10% higher than the one under tensile load (see Table 5).

In the case of the DD-POS profile, a comparable deformation capability of the specimens in tension and compression can be observed, with mild differences in the post-elastic

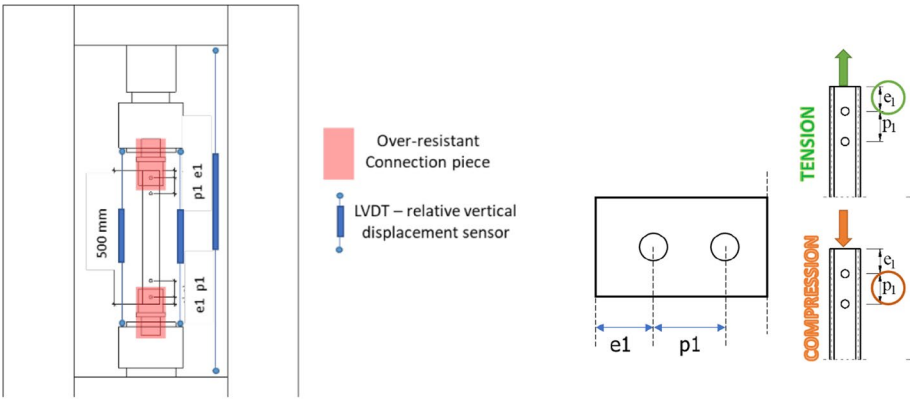


**Fig. 10** Test set up adopted for the tested diagonals: **a** configuration of the universal machine, **b** governing geometrical parameters based on the applied load

**Table 4** Main characteristics of the tested diagonals

| Case study structure | DD-POS | MD-POS |
|---|---|---|
| Diagonal cross-section shape | C | C |
| Thickness [mm] | 2.0 | 1.5 |
| Holes diameter | Ø13 | Ø13 |
| Bolt-diameter and class | M12 8.8 | M12 8.8 |
| $e_1$ | 29 | 20 |
| $p_1$ | 39 | 30 |
| Steel grade | S350 GD | S280 GD |
| Characteristic yield strength, $f_{yk}$ [MPa] | 350 | 280 |
| Characteristic ultimate strength, $f_{uk}$ [MPa] | 420 | 360 |
| Upper yield strength, $R_{eH}$ [MPa] (EN 10002-1 2001) | 480 | 530 |
| Tensile strength, $R_m$ [MPa] (EN 10002-1 2001) | 501 | 541 |

**Table 5** Maximum loads in tension

| Diagonal | Max tensile load [kN] | Max compressive load [kN] | Ratio C/T |
|---|---|---|---|
| DD-POS | 51.31 | 51.79 | 1.01 |
| MD-POS | 16.77 | 20.74 | 1.24 |

behaviour. Looking at Fig. 12a, b, considerable plastic deformation follows the exceedance of the nominal "yield" bearing strength of the bolt holes in both cases, accompanied by local buckling of the section web that is very pronounced in the case of the compression load.

In the case of the MD-POS profile, a comparable maximum force under tension and compression is obtained; yet this is accompanied by considerably different post-elastic

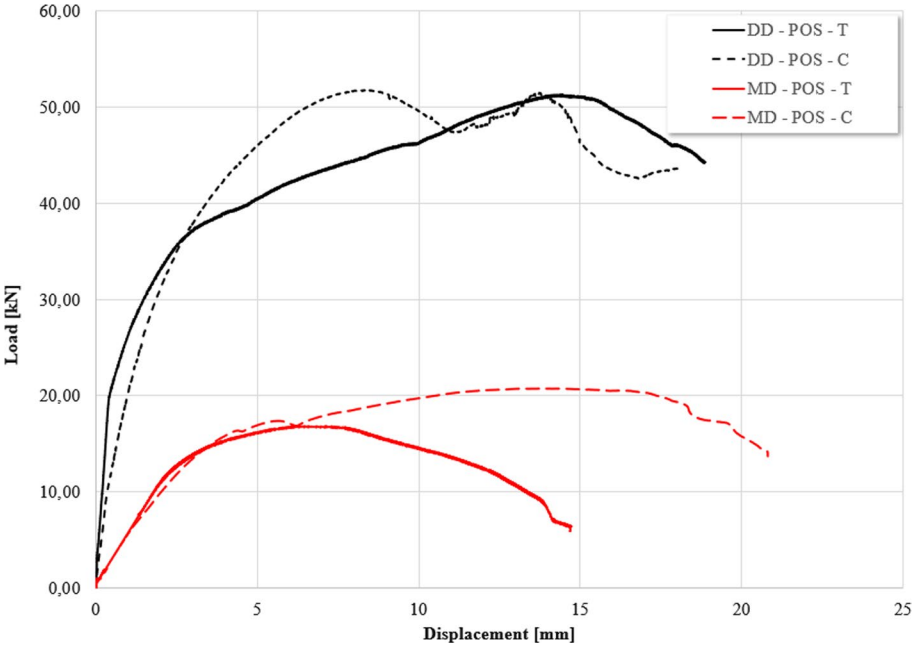


**Fig. 11** Experimental behaviour of the tested diagonals under tensile (T) and compressive (C) load


**Fig. 12** Final configuration of the tested elements, indexed by "T" for tension and "C" for compression

behaviour and deformation capabilities. This may be connected to the different failure mode observed in the two cases: under tensile load (Fig. 12c), the plastic ovalization "plateau" is followed by tearing of the end section of the element, which causes a drop in the resistance after reaching the peak load; under compression load (Fig. 12d), plastic ovalization produces a longer sustained plateau accompanied by local buckling of the profile.

Regarding the hysteretic behaviour of the connection, experimental tests performed by Natali et al. (2024) on diagonal-to-upright assemblies confirm the ductile behaviour observed in diagonal-only tests. For instance, Fig. 13 illustrates the monotonic and cyclic force–displacement curves of a test assembly comprising the DD-POS diagonal of Table 4. A good agreement is observed between the backbone of the cyclic and the monotonic curves, with negligible loss of strength and stiffness between the consecutive cycles. Due to the plastic ovalization of the diagonal bolt holes, the hysteretic loops are characterized by a highly pinched behaviour, which was taken into consideration during the numerical modelling presented in the following section.

### 3.3 Numerical modelling

The four structures were modelled using the OpenSees (McKenna et al. 2000) open-source software. To reduce the number of elements and degrees of freedom, the models were simplified using the methodology described in Tsarpalis et al. (2021a). Specifically, in the DD example the full cross-aisle frame was substituted with a pair of connected upright frames (i.e., one "macro-column") with calibrated horizontal springs at the top level, to simulate the stiffness of the roof. Similarly, in the MD case study a single upright frame was used instead of the 28 of the full model. A Rayleigh damping formulation was employed, using a viscous damping ratio of 3% for the first and second eigenperiods. In the double-depth case study a $G + Q$ combination for mass and gravity loads was employed, while a $G + 0.8{\cdot}Q$ for the multi-depth. The periods and mass participation factors of the four structures can be found in Table 6. The effect of pallet sliding was not considered in the analyses.

The uprights were simulated as elastic beam elements with a P-Δ formulation to account for the effect of geometric nonlinearities. In the standard design, material nonlinearities were not considered, as the elements and their connections are prone to brittle failure modes that cause swift collapse when initiated; thus, they were verified in post-processing. In the POS redesign, the only source of material nonlinearity was that of plastic ovalization of the diagonal bolt hole. The opening of the bolt hole was simulated using a zero-length element with an elastic-perfectly-plastic gap material, as illustrated in Fig. 14.

During loading (Points 1 to 3), the material behaves elastically with an elastic tangent $E_0$, until it reaches the yield force $F_y$; from this point onwards, it continues with a post-elastic (hardening) tangent $E_1$. The gap opens by the amount of plastic deformation the

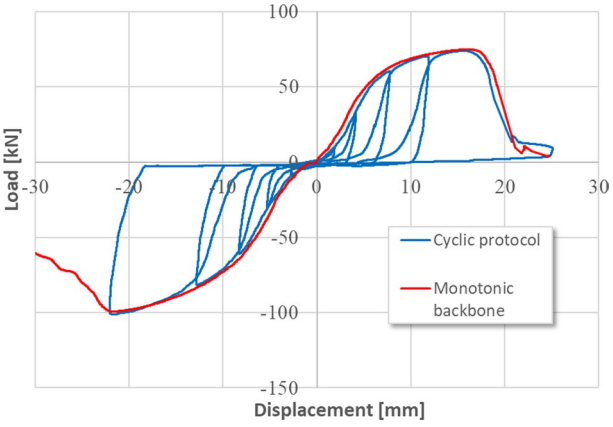


**Fig. 13** Force–displacement curve of a POS connection under cyclic loading (adopted from Natali et al. 2024)

**Table 6** Periods and mass participation factors for the case studies DD and MD according to the standard design (STD), and the POS redesign (POS)

| Mode # | DD-STD | | DD-POS | | MD-STD | | MD-POS | |
|---|---|---|---|---|---|---|---|---|
| | Period (sec) | Mass Part | Period (sec) | Mass Part | Period (sec) | Mass Part | Period (sec) | Mass Part |
| 1 | 2.60 | 68% | 2.46 | 69% | 1.58 | 63% | 1.31 | 63% |
| 2 | 0.97 | 11% | 0.85 | 17% | 0.51 | 17% | 0.42 | 19% |
| 3 | 0.53 | 5% | 0.45 | 6% | 0.26 | 5.4% | 0.21 | 5.6% |
| 4 | 0.35 | 3% | 0.30 | 2.8% | 0.18 | 1.8% | 0.15 | 1.4% |
| 5 | 0.25 | 1.2% | 0.21 | 1.3% | 0.14 | 0.7% | 0.11 | 1.0% |

material accumulates during the post-elastic phase (Points 2 to 3). Then, in the unloading branch, the material first unloads elastically to zero force (Points 3 to 4), and then it returns to its initial position with zero stiffness (Points 4 to 5) due to the gap opening. If load reversal occurs (Points 5 to 7), the same elastic-perfectly-plastic response is observed, and the gap opens also in the other direction of loading. From this point on, the material can bounce freely between Points 8 to 9 without developing any reaction force; it has to be subjected to a greater displacement (Point 10) to encounter any resistance while enlarging the gap. This flag-shaped force–deformation diagram is thus

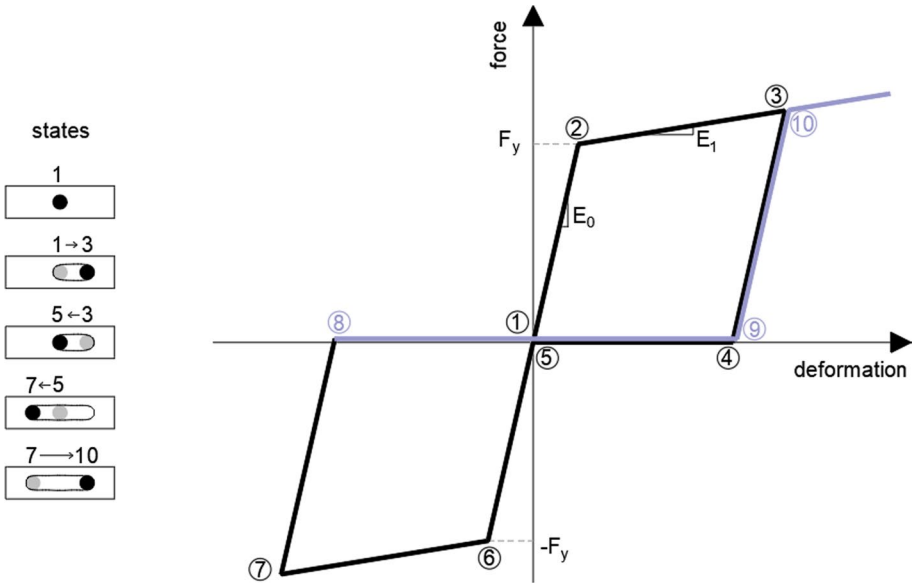


**Fig. 14** Simulating the plastic ovalization of a bolt hole under cyclic loading, using the elastic-perfectly-plastic gap material of OpenSees (McKenna et al. 2000). $F_y$ is the yield force, $E_0$ is the elastic tangent, and $E_1$ is the hardening tangent. The gap opens by the amount of plastic strain the material accumulates at each excursion. In the left side of the figure, the loading, unloading, and reloading states of the bolt hole are shown schematically, along with the numbered points corresponding to the right diagram (the gray and black circles indicate the initial and final position of the bolt, respectively)

characterized by significant pinching, which downgrades the amount of plastic energy the connection is capable of absorbing during a seismic excitation.

To determine the three parameters of the elastic-perfectly-plastic gap material ($F_y$, $E_0$, and $E_1$), a fitting procedure is followed. Recalling Fig. 6a, the bearing deformation of a steel material of grade lower than S460 (which is typical for diagonals on racking systems) follows a nonlinear path until it reaches 80% of the maximum bearing resistance (Može et al. 2021), i.e., up to point ($u_{80\%}$, $0.8{\cdot}F_{bR}$) in Fig. 15. It then continues with a constant slope up to full bearing resistance, i.e., point ($u_{xd}$, $F_{bR}$). From this point on it was assumed that it continues with zero stiffness until the bearing deformation is equal to *at least* one bolt diameter, $d$, beyond which significant loss of strength may occur. The overall fitting procedure is as follows (see Fig. 15):

(a) Find the elastic tangent of the gap material as: $E_0 = 0.8{\cdot}F_{bR}\,/u_{80\%}$.

(b) Find the optimal $F_y$ so that the hatched areas below and under the bilinear fit in Fig. 15 are approximately equal.

(c) Find the hardening tangent of the gap material as: $E_1 = (F_{bR} - F_y)\,/(d - F_y\,/\,E_0)$.

Note that: i) the above fitting procedure assumes that the force–deformation curve of prEN 1993-1-8:2021 (2021) is valid; ii) a symmetric cyclic behaviour is assumed, which is (theoretically) granted by rule POS 5 with the introduction of an empty hole that is adjacent to the bolt hole (i.e., by manipulating the $p_1$ parameter); iii) no cyclic degradation is considered in the connection. About point i), Fig. 16 shows the comparison between the analytical formulation of the connection behavior and the experimental one under tensile load. It can be noticed that the Eurocode formula is quite representative, especially for the DD-POS diagonal. Regarding the MD-POS one, the elastic part is well approximated, while the experimental test shows an over-resistance that the analytical model neglects. Nevertheless, this modelling

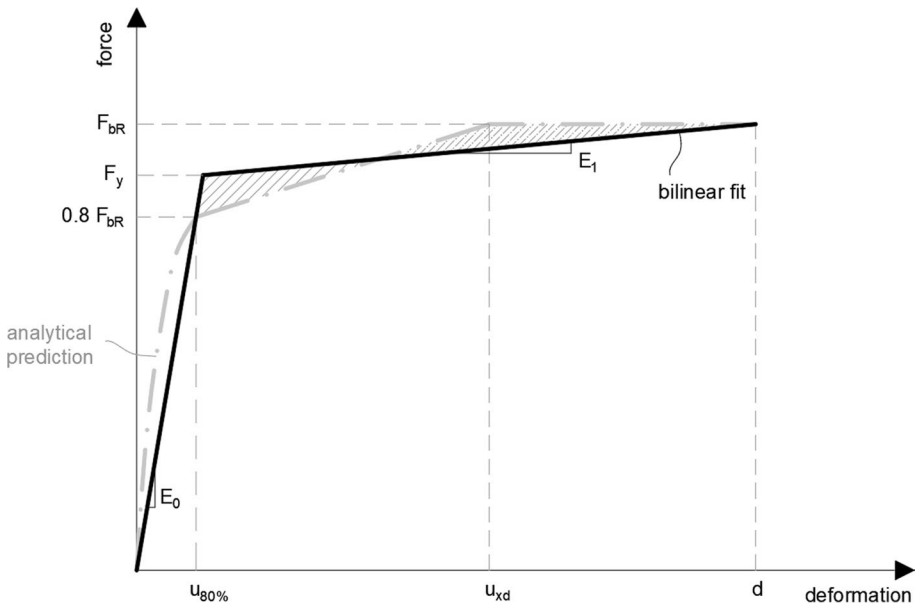


**Fig. 15** Fitting the parameters $F_y$, $E_0$, and $E_1$ of the elastic-perfectly-plastic gap material, to match the analytical predictions of (3), (4), and (5). $F_y$ is calculated so that the hatched areas below and under the bilinear fit are approximately equal

strategy can be surely adopted in this study, as it plays on the safe side for its purposes. About point ii), the outcomes of the preliminary experimental tests showed that the adoption of the additional hole surely helps in limiting the bearing resistance under compression. Finally, regarding point iii), cyclic tests do confirm its validity for properly designed POS connections (see Natali et al. 2024 and Fig. 13).

Even if further experimental studies are needed to assure a more accurate calibration, these preliminary tests showed that the adoption of the analytically defined behavior for the diagonal connection provides a good approximation and give the chance to evaluate the global pros and cons in the application of the POS strategy, which is the main purpose of this study.

After the determination of $F_y$, $E_0$, and $E_1$, the diagonal and its bolted ends can be simulated by a macro-element that comprises (a) a zero-length element with an elastic-perfectly-plastic gap material, and (b) an elastic beam element, as shown in Fig. 17. Instead of using two zero-length elements, one for each end of the diagonal, it is more efficient to use one and multiply the elastic and hardening tangents by 0.5, i.e., $0.5{\cdot}E_0$ and $0.5{\cdot}E_1$, respectively. $F_y$ is not modified as the two ends are identical springs in series.

A final modelling detail is related to the initial shear stiffness of the upright frame, which is significantly reduced due to the deformation of the braces and their ends, as well as the slipping and bending of the bolts (Talebian et al. 2018). This phenomenon is typically considered in a beam element model by employing an axial spring in series with the diagonal. This spring has a stiffness of $K_{tot}$, calibrated by experimental shear tests. One may break down $K_{tot}$ into two springs in series, one is the aforementioned elastic-perfectly-plastic gap element that accounts for the bearing deformation and has elastic stiffness $0.5{\cdot}E_0$, and the other should account for all the other factors that contribute to the shear stiffness of the upright frame. Thus, this second spring should have an axial stiffness of $(0.5{\cdot}E_0{\cdot}K_{tot})\ /\ (0.5{\cdot}E_0 - K_{tot})$. Instead of using these two springs, it was more efficient to use only the one that accounts for the bearing deformation, and implicitly consider the other by reducing numerically the cross-section area of the diagonal element to a value of $A\prime$ (Fig. 17) as follows:

$$A\prime = \frac{A \cdot L \cdot E_0 \cdot K_{tot}}{A \cdot E \cdot E_0 - 2 \cdot A \cdot E \cdot K_{tot} + L \cdot E_0 \cdot K_{tot}} \tag{13}$$

where $E$, $A$, $L$, is the Young's modulus, gross cross-section area, and length of the diagonal elements, respectively.

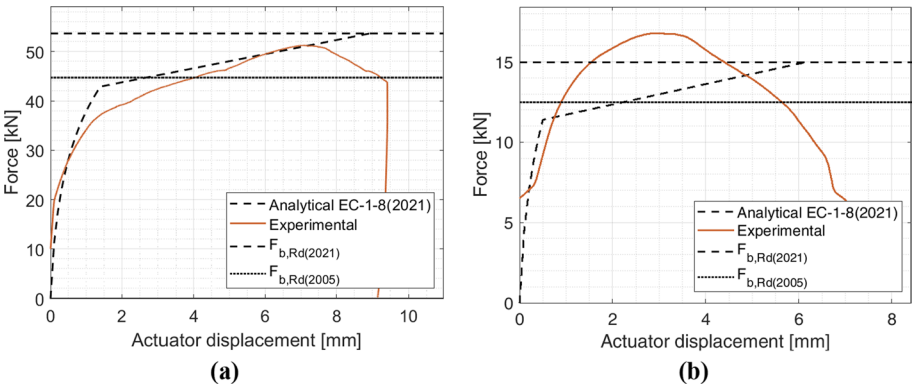


**Fig. 16** Analytical versus experimental behaviour of the connection under tensile load for the (a) DD-POS element and (b) MD-POS diagonal

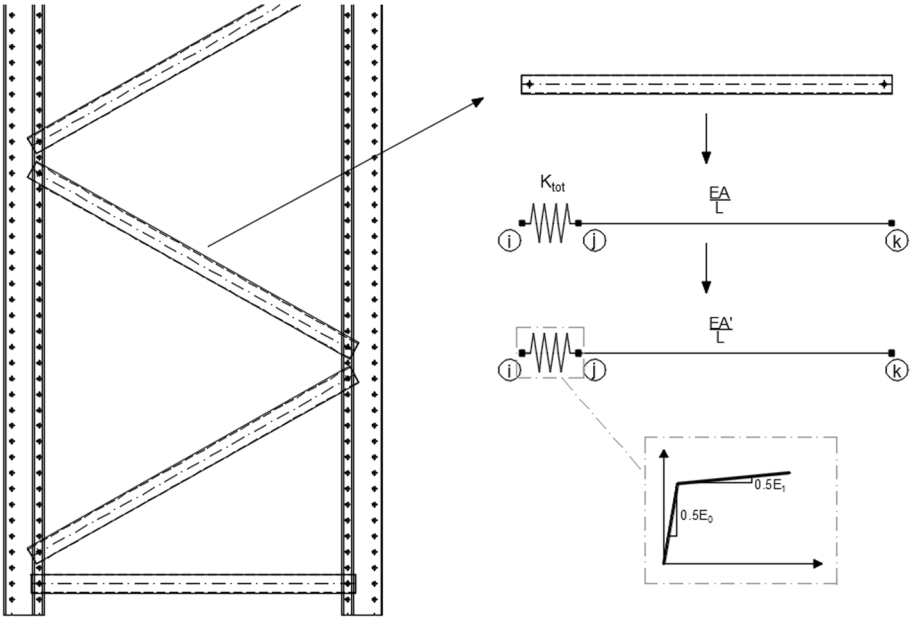


**Fig. 17** Numerical modelling of a diagonal element with bearing failure behaviour in OpenSees (McKenna et al. 2000). Nodes i and j are connected by a zero-length element with an elastic-perfectly-plastic gap material, and nodes j and k by an elastic beam element with stiffness $EA\prime / L$. The cross-section area of the beam element is numerically reduced to $A\prime$ in order to achieve the elastic shear stiffness of the upright frame taken from experimental shear tests

### 3.4 Seismic assessment of case studies

To compare the two design approaches, a multi stripe analysis (Jalayer and Cornell 2009) was performed for each case study, employing 30 natural records from the PEER-NGA strong motion database (Ancheta et al. 2013) that match the 10% in 50 yr conditional spectrum (Baker 2010; Lin et al. 2013a, 2013b) of Van in Turkey, using the geometric mean of spectral acceleration *AvgSa* as the intensity measure (IM) (Kohrangi et al. 2017). The set is available at Kohrangi et al. (2018). The records were scaled to six IM levels that correspond to 60%, 30%, 20%, 10%, 5%, and 3% in 50 years probability of exceedance. Additionally, all records were pre-multiplied by the design spectrum modification factor $E_{D3}$. While one may be reluctant regarding the actual value of $E_{D3}$ (as it is based on shaking table tests or post-earthquake surveys of racks that are non-ARSW-like), to achieve a fair assessment of the designs at the design-level intensity (i.e., the 20% in 50 years stripe), a uniform value of $E_{D3} = 0.8$ (see Table 1) was considered.

In the numerical models of the standard design, a post-processing procedure was followed to derive the utilization factor, *UF*, of (a) the steel members using the verification checks given in EN 1993-1-1 (2005), EN 1993-1-3 (2006), and EN 15512 (2009), (b) the steel bolted connections using EN 1993-1-8 (2005), and (c) the base plates with bonded anchors using EN 1992-4 (2018). All design resistances were multiplied by a factor of 1.1, which roughly approximates the available overstrength of the structure, in order to derive expected rather than design values. Due to the prevalence of brittle failure modes in

standard designs, it was assumed that the failure of any member/connection (i.e., when a *UF* exceeds the threshold value of 1.0) leads to a global collapse of the structure.

In the "POS" numerical models, the diagonal-to-upright connection was modelled using the nonlinear zero-length element of Fig. 17. While deriving its force–deformation curve (Fig. 15), $F_{bR}$ was calculated by omitting the safety factor $\gamma_{M2}$ in (1), again targeting expected rather than design values. Note that bearing failure typically demonstrates high overstrength ratios and the use of the design bearing resistance ($F_{bRd}$) would have possibly resulted in lower seismic demands to the non-dissipative components of the structure. An additional global collapse rule was considered: if the gap displacement of the zero-length element exceeds the value of $1.1 \cdot d_0$, then it is assumed that the loss of strength in the connection and subsequent deformation are so large that the upright frame loses its global stability. The rest of the structural components were modelled and verified similarly to the standard design.

Figure 18 illustrates the maximum derived *UF* s for case study DD, utilizing two arbitrary records from the set scaled at the 10% in 50 years intensity. For each record, the results of two response history analyses are shown: these corresponding to the standard (DD-STD) and the POS design (DD-POS), respectively. The *UF* s of the structural members (lines) and the connections (circles) are grouped into six performance intervals, each assigned a distinct colour. Moreover, the figures contain the maximum *UF* values for the entire group of uprights (UP), diagonals (DG), anchors (AN), and diagonal-to-upright connections (OV).

Both records show similar patterns: The bottommost members and connections experienced high *UF* values, while the upper half of the structure demonstrated moderate involvement in the global failure mechanism. For the standard design and the first record (Hector Mine 1999), failures occurred in the anchored connections ($UF = 151\%$) and the bottom diagonals ($UF = 102\%$), while the uprights were stressed to a maximum $UF = 84\%$. Contrarily, the POS structure averted both failure modes by exploiting the ductility of the diagonal ends, which deformed to a maximum *UF* of 84% (i.e., maximum recorded deformation over maximum allowed deformation). The second record (Chi-Chi Aftershock 1999) illustrates a scenario where the POS design kept at bay both the upright buckling and anchor failure modes that occurred in the standard model, however mildly excessive deformations were recorded in the bottom diagonals ($UF = 110\%$).

Likewise, Fig. 19 displays the maximum *UF* s for case study MD using two different ground motions than those depicted in the analysis of rack DD. In this example, the upper half of the upright frames participated more actively in the global failure mechanism, which is reflected by the high *UF* s of the top-level diagonals and uprights. This behaviour is attributed to the increased stiffness of the roof truss in case study MD, which resulted in a structural behaviour that deviated from that of a classical cantilever. In the first record, the standard design experienced anchor failure, accompanied by near-failure *UF* s in the bottom uprights and diagonals. The implementation of the POS design effectively safeguarded the base connections and reduced the *UF* s in the uprights by 16%. Improved behaviour was also observed in the second record, where the standard design suffered from component failures along the entire height of the structure, while the POS rack prevented all brittle failure modes and managed to exploit the ductility of both the bottom and the upper diagonal connections.

Figure 20a summarizes the results of the multi stripe analysis for case study DD, using pie charts to compare the two designs. The pie charts show the number of times a failure mode was observed in each stripe of analyses; if multiple failure modes were observed for a single record, the one with the highest utilization (i.e.,

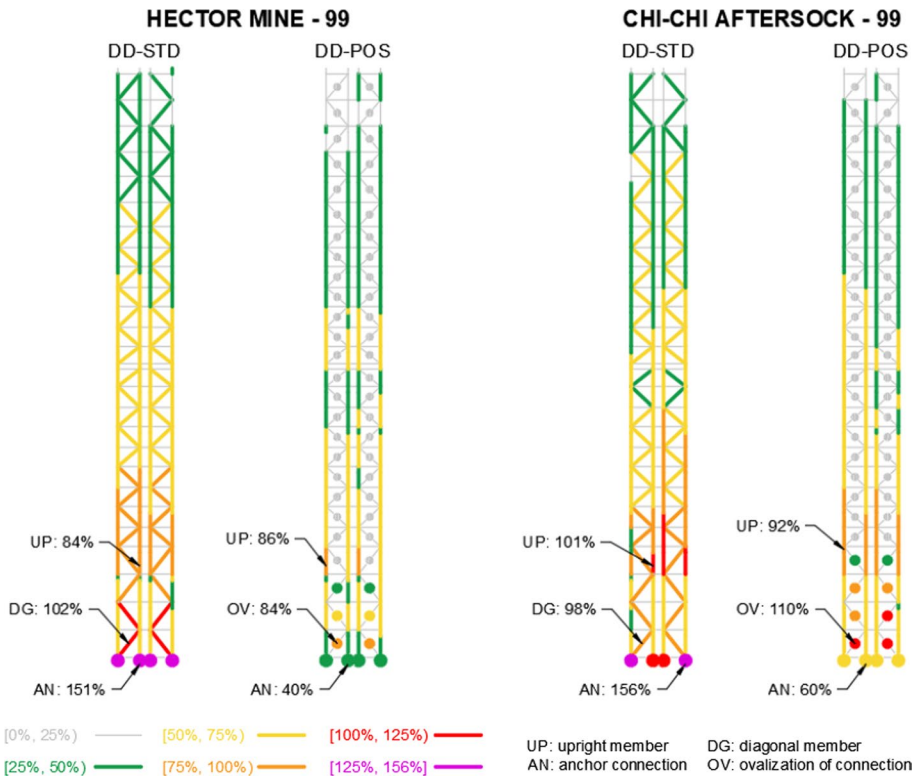


**Fig. 18** Maximum utilization factors for the structural members (lines) and connections (circles) of case study DD, for two records scaled at the 10% in 50 years intensity: Hector Mine 1999, Station ARLETA-NORDHOFF, PEER NGA2 (left) and Chi-Chi Aftershock 1999, Station CHY054, PEER NGA2 (right)

demand-to-capacity) factor is considered. As expected, both designs performed excellently at the two lowest scales, with very few records leading to a component failure. At the design level (i.e., the 20% in 50 years stripe), 7 and 1 out of the 30 records had a component failure in the standard and the POS models, respectively, showing a clear advantage of the latter. The difference between the two designs is also pronounced at probabilities of exceedance lower (i.e., higher intensities) than the design level. For instance, at the 10% in 50 years stripe, which is the design level for regular steel buildings, POS achieved a 32% increase of non-collapse records. Still, at the highest IM scales, the utilization factors on the uprights exceeded the threshold value of 1.0 even in the POS design, despite the reduction of seismic forces due to the ovalization of the diagonal bolt hole.

Accordingly, Fig. 20b shows the results of the multi stripe analysis for case study MD. POS was again capable of completely preventing the diagonals and the anchorage system from failing and scored better results for all IM levels. At the design-level stripe, 16 and 3 out of the 30 records led to a component failure in the standard and the POS models, respectively, highlighting a remarkable improvement in the seismic performance of the upright frames. However, upright buckling was still prevalent at high IMs, which indicates that rule POS 8 only partially creates over-resistant columns. In

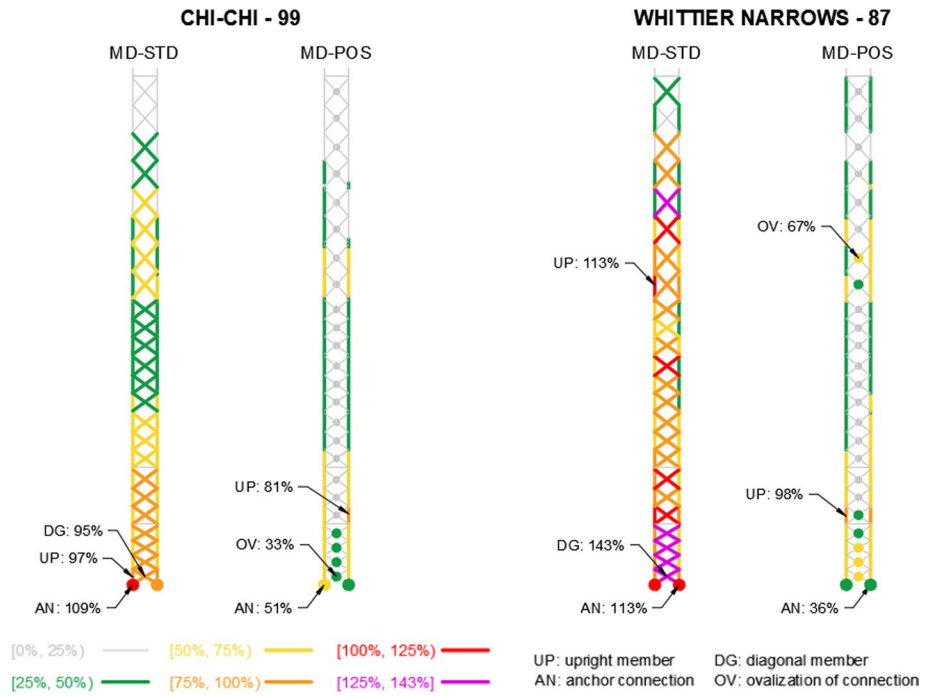


**Fig. 19** Maximum utilization factors for the structural members (lines) and connections (circles) of case study MD, for two records scaled at the 10% in 50 years intensity: Chi-Chi 1999, Station CHY029, PEER NGA2 (left) and Whitter Narrows 1987, Station ALHAMBRA FREMONT, PEER NGA2 (right)

this sense, stricter capacity design rules could be used on the uprights, similar to those of EN 1998-1 (2004), with the obvious drawback of increasing the overall cost of the racking structure.

Note that ARSWs designed according to POS can perform adequately well even if the available global and local overstrength is low (e.g., $\Omega = 1.1$ used herein) due to the structural optimization performed by professionals. In this sense, the $q = 1.8$ used in the POS design comprises a lower-bound value that can be improved after the consideration of laboratory test data and the calibration of the models per the INNOSEIS approach (Tsarpalis et al. 2020; Vamvatsikos et al. 2020). Consequently, the pie-charts produced for the POS case-studies are essentially the first step in this calibration process, as they clearly indicate that the q-values selected are more than good enough (and could actually be increased) if the aim is to provide the same level of safety that currently designed ARSWs have. Indeed, if it assumed that the safety espoused by EN16681 (2016) is adequate, then the results at the design-level stripes show that the q-factor can be increased to 2.0 or 2.5 at least. If, instead, one decides that the bar needs to be raised to ensure higher safety for the highly-valuable ARSWs compared to more typical APR designs (which are after all the subject of EN16681), then this $q = 1.8$ may only receive some modest calibration.

Finally, one may observe that the MD example demonstrated an inferior seismic performance with respect to the DD, in both standard and POS designs. This was attributed to the different assumptions adopted during their seismic design and to the fact that DD employed a more uniform distribution of $\Omega$ factors on the diagonals, by dividing

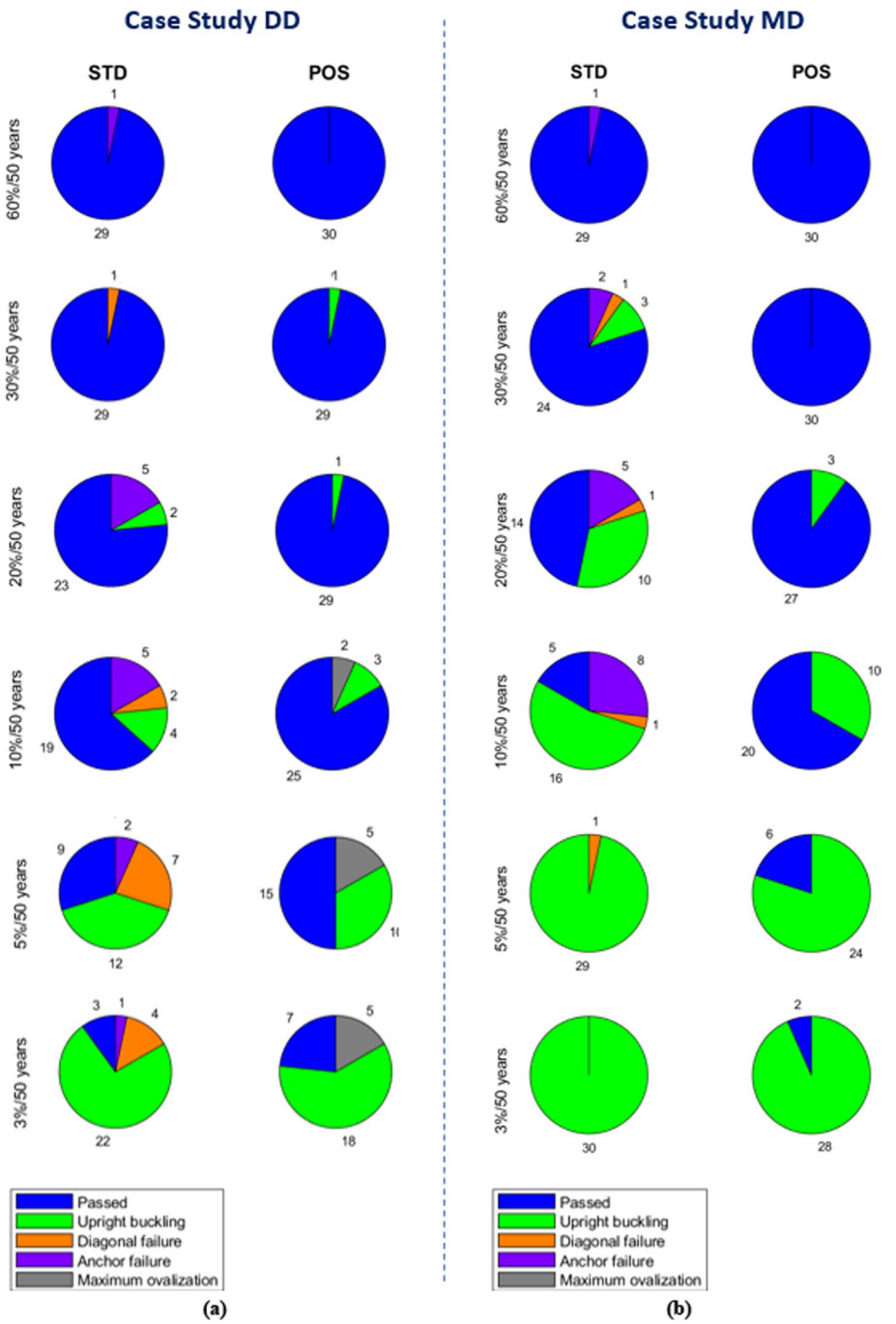


**Fig. 20** Multi stripe analysis for (a) the double-depth rack (DD) and (b) the multi-depth rack (MD), using a set of 30 records scaled to six IM levels. Two pie charts are given per case study and stripe, showing the number of times a failure mode was observed on the standard (left) and the POS (right) design. If multiple failure modes were observed on a single record, the one with the highest utilization factor is considered

them into four groups along the vertical direction. While this smooth reduction of the diagonals' resistance was not explicitly imposed by the capacity design rules POS 1 to POS 10, it potentially leads to a more uniform exploitation of structural ductility, and thus, to an improved seismic behaviour.

## 4 Conclusions

A state-of-the-art seismic design strategy for the cross-aisle direction of racking systems has been presented, namely the plastic ovalization strategy (POS). In contrast to the "non-dissipative" approaches adopted by the current seismic codes, POS aims to increase the ductility of the individual upright frames while preserving the simple connections and light steel members used in conventional racks. This is achieved by tasking the bearing deformation of the diagonal bolt hole to absorb seismic deformations, while the rest structural components are designed to be over-resistant by employing new capacity design rules.

To assess the performance of POS from the design and assessment standpoint, the cross-aisle frames of one double-depth and one multi-depth ARSW were examined. Each case study was designed twice by an expert in the racking technology, once using conventional design approaches and then by additionally employing the proposed POS rules. During the redesign it was observed that the cross-sections of the uprights were slightly modified while in some cases lighter diagonals were employed, which indicates that by employing POS the overall cost of the structure does not necessarily increase.

Consequently, the two design solutions were compared by conducting a multi stripe analysis using a set of 30 hazard-consistent records. In the POS models, the plastic ovalization mechanism of the bolt hole was simulated using a zero-length element with an elastic-perfectly-plastic gap material, calibrated on the analytical formulation for the bearing resistance provided by the prEN 1993-1-8: 2021 (2021). This behaviour has been compared with the one experimentally obtained for the same diagonals adopted in the case studies, showing the capability of such a formulation to approximate well the actual behaviour, at least for monotonic loads. However, further experimental activity is required for a full validation of the method and to extend the calibration to all diagonal shapes and thicknesses, while investigating also the behavior obtained in particular cases (e.g., very low thickness profiles, mixed plastic ovalization-tearing of the end section failures). The results of the seismic assessment showcased a distinct advantage of the POS design. Even when limited global and local overstrength was assumed due to structural optimization, the redesigned racks demonstrated the desired behaviour at the design level with only few records leading to brittle failure modes. This enhanced behaviour was also observed for stripes higher than the design level ones; however, for high IMs upright buckling was prevalent. Overall, POS promises to increase the resilience of racking systems in an economic and efficient way and sets the ground for a performance-based earthquake design of racks, in tandem with the current trends in the earthquake engineering community.

**Funding** Open access funding provided by HEAL-Link Greece. The authors acknowledge the financial support provided by the European Commission through the Research Fund for Coal and Steel (RFCS) Project STEELWAR, under Grant Agreement Number 754102.

**Availability of data and materials** Some or all data, models or code that support the findings of this study are available from the corresponding author upon reasonable request.

## Declarations

**Conflict of interest** The authors declare that they have no conflict of interests.



## References

Ancheta TD, Darragh RB, Stewart JP, Seyhan E, Silva WJ, Chiou BSJ, Wooddell KE, Graves RW, Kottke AR, Boore DM, Kishida T, Donahue JL (2013) PEER NGA-West2 Database, Technical Report PEER 2013/03. Pacific Earthquake Engineering Research Center, Berkeley, CA

ANSI/AISC 360-16 (2016) Specification for structural steel buildings, Chicago, Illinois, USA

ASCE/SEI 7-22 (2022) Minimum design loads and associated criteria for buildings and other structures, American Society of Civil Engineers, Reston, Virginia. https://doi.org/10.1061/9780784415788

Baker JW (2010) Conditional mean spectrum: tool for ground-motion selection. J Struct Eng. https://doi.org/10.1061/(ASCE)ST.1943-541X.0000215

Brandonisio G, Toreno M, Grande E, Mele E, De Luca A (2012) Seismic design of concentric braced frames. J Constr Steel Res 78:22–37. https://doi.org/10.1016/j.jcsr.2012.06.003

Caprili S, Morelli F, Salvatore W, Natali A (2018) Design and analysis of automated rack supported warehouses. Open Civ Eng J 12(1):150–166. https://doi.org/10.2174/1874149501812010150

Draganić H, Dokšanović T, Markulak D (2014) Investigation of bearing failure in steel single bolt lap connections. J Constr Steel Res 98:59–72. https://doi.org/10.1016/j.jcsr.2014.02.011

EN 10002-1 (2001) Metallic materials—tensile testing—part 1: method of test at ambient temperature, European Committee for Standardization (CEN), Brussels, Belgium

EN 15512 (2009) Steel static storage systems—adjustable pallet racking systems—principles for structural design, European Committee for Standardization (CEN), Brussels, Belgium

EN 16681 (2016) Steel static storage systems—adjustable pallet racking systems—principles for seismic design, European Committee for Standardization (CEN), Brussels, Belgium

EN 1993-1-1 (2005) Eurocode 3: design of steel structures—part 1-1: general rules and rules for buildings, European Committee for Standardization, Brussels, Belgium

EN 1993-1-3 (2006) Eurocode 3: design of steel structures—part 1–3: general rules—supplementary rules for cord-formed members and sheeting, European Committee for Stand-ardization, Brussels, Belgium

EN 1993-1-8 (2005) Eurocode 3: design of steel structures—part 1-8: design of joints, European Committee for Standardization, Brussels, Belgium

EN 1998-1 (2004) Eurocode 8: design of structures for earthquake resistance—part 1: general rules, seismic actions and rules for buildings, European Committee for Standardi-zation, Brussels, Belgium

EN 1992-4 (2018) Eurocode 2: Design of concrete structures - Part 4: Design of fastenings for use in concrete, European Committee for Standardization, Brussels, Belgium

Fülöp LA, Dubina D (2004) Performance of wall-stud cold-formed shear panels under monotonic and cyclic loading: part I: experimental research. Thin-Walled Struct 44(2):321–338. https://doi.org/10.1016/S0263-8231(03)00063-6

Galli P, Castenetto S, Peronace E (2012) The MCS macroseismic survey of the Emilia 2012 earthquakes. Ann Geophys 55:663–672. https://doi.org/10.4401/ag-6163

Jalayer F, Cornell CA (2009) Alternative non-linear demand estimation methods for probability-based seismic assessments. Earthq Eng Struct Dyn 38(8):951–972. https://doi.org/10.1002/eqe.876

Kiymaz G (2009) Investigations on the bearing strength of stainless steel bolted plates under in-plane tension. Steel Compos Struct 9(2):173–189. https://doi.org/10.12989/scs.2009.9.2.173

Kohrangi M, Bazzurro P, Vamvatsikos D, Spillatura A (2017) Conditional spectrum-based ground motion record selection using average spectral acceleration. Earthq Eng Struct Dyn 46(10):1667–1685. https://doi.org/10.1002/eqe.2876

Kohrangi M, Tsarpalis D, Vamvatsikos D (2018) CS(AvgSA) consistent Records and Hazard curves for Van and Montopoli. STEELWAR Project. Link: http://users.ntua.gr/divamva/resources/Van_set_10_50yrs.rar

Kondratenko A, Kanyilmaz A, Castiglioni CA, Morelli F, Kohrangi M (2022) Structural performance of automated multi-depth shuttle warehouses (AMSWs) under low-to-moderate seismic actions. Bull Earthq Eng 20:1247–1295. https://doi.org/10.1007/s10518-021-01193-y

Landolfo R (2019) Lightweight steel framed systems in seismic areas: current achievements and future challenges. Thin-Walled Struct 140:114–131. https://doi.org/10.1016/j.tws.2019.03.039

Lin T, Haselton CB, Baker JW (2013a) Conditional spectrum-based ground motion selection. Part I: hazard consistency for risk-based assessments. Earthq Eng Struct Dyn 42(12):1847–1865. https://doi.org/10.1002/eqe.2301

Lin T, Haselton CB, Baker JW (2013b) Conditional spectrum-based ground motion selection. Part II: intensity-based assessments and evaluation of alternative target spectra. Earthq Eng Struct Dyn 42(12):1867–1884. https://doi.org/10.1002/eqe.2303

McKenna F, Fenves GL, Scott MH, Jeremic B (2000) Open system for earthquake engineering simulation (OpenSees). University of California, Berkeley, CA, Pacific Earthquake Engineering Research Center

Može P, Beg D (2014) A complete study of bearing stress in single bolt connections. J Constr Steel Res 95:126–140. https://doi.org/10.1016/j.jcsr.2013.12.002

Može P, Yang F, Veljkovic M (2021) Validation and application of bearing and block tearing resistance; background to prEN1993–1–8:2021. J Constr Steel Res. https://doi.org/10.1016/j.jcsr.2021.106985

Natali A, Morelli F (2023) Experimental validation of dissipative reduced-section thin walled diagonals for seismic-resistant Automated Rack Supported Warehouses. Procedia Struct Integr 44:2334–2341. https://doi.org/10.1016/j.prostr.2023.01.298

Natali A, Morelli F, Salvatore W (2022a) On the seismic design and behavior of automated rack supported warehouses. Bull Earthq Eng 21:1081–1115. https://doi.org/10.1007/s10518-022-01566-x

Natali A, Morelli F, Salvatore W (2022b) Seismic performance of dissipative automated rack supported warehouses. In: The 8th European congress on computational methods in applied sciences and engineering (ECCOMAS 2022)

Natali A, Morelli F, Salvatore W (2022c) Influence of the design parameters on the current seismic design approach for Automated Rack Supported Warehouses. In: 7th World congress on civil, structural, and environmental engineering (CSEE'22)

Natali A, Morelli F, Salvatore W (2022d) Seismic performance of currently designed Automated Rack Supported Warehouses. In: 7th World congress on civil, structural, and environmental engineering (CSEE'22)

Natali A, Morelli F, Vulcu M, Tsarpalis D, Vamvatsikos D, Salvatore W, Hoffmeister B, Vayas I (2024) Experimental Behaviour of ductile diagonal connections for rack supported warehouses. Bull Earthq Eng (under review)

prEN 1993-1-8 (2021) Eurocode 3: Design of Steel Structures—Part 1–8: Design of joints, European Committee for Standardization, Brussels, Belgium

RMI, ANSI MH16.1.12 (2012) Specification for the design, testing and utilization for industrial steel storage racks, Rack Manufacturer's Institute, Charlotte, NC

STEELWAR (2017) Advanced structural solutions for automated STEELrack supported WARehouses, The Steelwar Project Consortium, Pisa, Italy. https://www.unipi.it/index.php/risultati-e-prodotti/item/10663-steelwar

Stojadinovic B, Tipping S (2007) Structural testing of corrugated sheet steel shear walls, Research report, Berkeley, University of California

Tagliafierro B, Montuori R, Vayas I, Antonodimitraki S, Titirla MD, Simoncelli M, Lignos X (2021) Experimental testing campaign and numerical modelling of an innovative base-plate connection for pallet racking systems. In: International conference on computational methods in structural dynamics and earthquake engineering (COMPDYN) 2021. https://doi.org/10.7712/120121.8687.19514

Talebian N, Benoit PG, Baldassino N, Karampour H (2018) Factors contributing to the transverse shear stiffness of bolted cold-formed steel storage rack upright frames with channel bracing members. Thin-Walled Struct 136:50–63. https://doi.org/10.1016/j.tws.2018.12.001

Tsarpalis P, Bakalis K, Thanopoulos P, Vayas I, Vamvatsikos D (2020) Pre-normative assessment of behaviour factor for lateral load resisting system FUSEIS pin-link. Bull Earthq Eng 18:2681–2698. https://doi.org/10.1007/s10518-020-00799-y

Tsarpalis D, Vamvatsikos D, Vayas I (2021a) Seismic assessment approaches for mass-dominant sliding contents: the case of storage racks. Earthq Eng Struct Dyn 51(4):812–831. https://doi.org/10.1002/eqe.3592

Tsarpalis D, Vamvatsikos D, Vayas I, Delladonna F (2021b) Simplified modelling for the seismic performance assessment of automated rack-supported warehouses. J Struct Eng. https://doi.org/10.1061/(ASCE)ST.1943-541X.0003153

Tsarpalis D, Vamvatsikos D, Deladonna F, Fabini M, Hermanek J, Dot MP, Sesana S, Vantusso E, Vayas I (2022) Macro-characteristics and taxonomy of steel racking systems for seismic vulnerability assessment. Bull Earthq Eng. https://doi.org/10.1007/s10518-022-01326-x

Vamvatsikos D, Bakalis K, Kohrangi M, Pyrza S, Castiglioni C, Kanyilmaz A, Morelli F, Stratan A, D' Aniello M., Calado L., Proença J.M., Degee H., Hoffmeister B., Pinkawa M., Thanopoulos P., Vayas I. (2020) A risk-consistent approach to determine EN1998 behaviour factors for lateral load resisting systems. Soil Dyn Earthq Eng. https://doi.org/10.1016/j.soildyn.2019.106008

Vigh LG, Deierlein GG, Miranda E, Liel AB, Tipping S (2013) Seismic performance assessment of steel corrugated shear wall system using non-linear analysis. J Constr Steel Res 45:48–59. https://doi.org/10.1016/j.jcsr.2013.02.008

Vigh LG, Liel AB, Deierlein GG, Miranda E, Tipping S (2014) Component model calibration for cyclic behavior of a corrugated shear wall. Thin-Walled Struct 75:53–62. https://doi.org/10.1016/j.tws.2013.10.011